An improved anisotropy-resolving subgrid-scale model with the aid of a scale-similarity modeling concept

ABE, Ken-ichi
Department of Aeronautics and Astronautics, Faculty of Engineering, Kyushu University : Professor

出版情報：International Journal of Heat and Fluid Flow. 39, pp.42-52, 2013-02. Elsevier
バージョン：
権利関係：

An improved anisotropy-resolving subgrid-scale model with the aid of a scale-similarity modeling concept

Ken-ichi Abe[1]

[1] *Department of Aeronautics and Astronautics, Kyushu University, Fukuoka, Japan*

Abstract

An improved subgrid-scale (SGS) model was proposed by combining an isotropic linear eddy-viscosity term with an extra anisotropic term. In the present study, primary attention was given to maintaining the computational stability while improving the predictive performance particularly for coarse grid resolution in the near-wall region. For the extra anisotropic term used for this purpose, the present study introduced a residual term after subtracting an eddy-viscosity form from the Bardina SGS-Reynolds-stress model (Bardina et al., AIAA Paper, 80-1357, 1980). The resultant extra term yields no undesirable extra energy transfer between the grid-scale and SGS components that could cause numerical instability under coarse grid conditions. Therefore, this extra term is not expected to have any serious negative effects on the computational stability. In order to assess the performance, the proposed model was applied to the numerical simulation of fully-developed plane channel flows with various grid resolutions and at various Reynolds numbers. The computational results were considerably improved by the present SGS model and detailed investigations of the obtained results indicated the usefulness of the present model for engineering applications.

Keywords:
Turbulence, Large-eddy simulation, SGS-stress anisotropy,
Scale-similarity model, Near-wall turbulent structure

Nomenclature

k_{SGS}	SGS turbulence energy
$\overline{P}$	filtered static pressure
R'_{ij}	SGS-stress anisotropy expression
Re_τ	Reynolds number based on friction velocity and half channel height
S_{ij}	strain-rate tensor, $\left(\partial\overline{U}_i/\partial x_j + \partial\overline{U}_j/\partial x_i\right)/2$
t	time
$\overline{U}$	filtered velocity in x-direction
$\overline{U}_i, u_i$	filtered velocity and fluctuation in i-direction, respectively
u, v	fluctuation in x- and y-directions, respectively
u_τ	friction velocity
x, y, z	Cartesian coordinates
x_i	Cartesian coordinate in i-direction
$(\ )^+$	normalized value by friction velocity
$\overline{(\ )}$	filtered value
$\widehat{(\ )}$	test-filtered value

Greek symbols

δ	half channel height
Δ	SGS filter width
ε_{SGS}	dissipation rate of SGS turbulence energy
ν, ν_{SGS}	kinematic and SGS eddy viscosities, respectively
ρ	density
τ_{ij}	SGS-stress tensor
Ω_{ij}	vorticity tensor, $\left(\partial\overline{U}_i/\partial x_j - \partial\overline{U}_j/\partial x_i\right)/2$

1. Introduction

Large eddy simulation (LES) is a useful method for predicting complex turbulence in engineering applications. In LES, the grid-scale (GS) eddies are directly resolved, while the subgrid-scale (SGS) eddies must be modeled. The governing equations for an incompressible turbulence may be written as

$$\frac{\partial \overline{U}_i}{\partial x_i} = 0,$$

$$\frac{\mathrm{D}\overline{U}_i}{\mathrm{D}t} = -\frac{1}{\rho}\frac{\partial \overline{P}}{\partial x_i} + \frac{\partial}{\partial x_j}\left\{\nu\left(\frac{\partial \overline{U}_i}{\partial x_j} + \frac{\partial \overline{U}_j}{\partial x_i}\right) - \tau_{ij}\right\}, \tag{1}$$

where $\overline{(\ \ )}$ denotes a filtered value. In Eq. (1), ρ, $\overline{P}$, $\overline{U}_i$ and ν denote the density, the filtered static pressure, the filtered velocity, and the kinematic viscosity, respectively. The SGS-stress tensor τ_{ij} is originally expressed as $\tau_{ij} = \overline{U_i U_j} - \overline{U}_i \overline{U}_j$.

Generally speaking, LES requires far fewer grid nodes than does direct numerical simulation (DNS). However, this is still an enormous requirement for engineering applications at high Reynolds number (Re). It is well known that a reasonable LES for a channel flow requires a grid resolution such as $\Delta x^+ \sim 100$ (x: the streamwise direction), $\Delta z^+ \sim 20$ (z: the spanwise direction) and $\Delta y^+ \sim 1$ (y: the wall-normal direction) in the near-wall region. Note that $(\ \ )^+$ denotes a value normalized by the friction velocity u_τ. In general, it becomes more and more difficult to achieve this required grid resolution as the flow Reynolds number increases, especially in the spanwise (cross-stream) direction.

For an LES to be reasonable, it is essential to guarantee a grid resolution at least as fine as the scale of a large (energy-containing) eddy. This condition is generally achieved in the region far from the wall, but cannot be guaranteed in the near-wall region of high-Re turbulent flows, where the dominant eddies become smaller and smaller. Although we often encounter such severe computational conditions in practical engineering applications, the predictive performance of existing SGS models is not always satisfactory. Therefore, if it is possible to provide a modeling strategy to cover such severe conditions, it will become a useful option from an engineering viewpoint.

The present paper contributes to the ongoing search for a better SGS model that is applicable to complex high-Re turbulent flows. The emphasis of the present contribution is on the introduction of an advanced effective

modification into an SGS-stress expression. The present SGS model is constructed by combining a representative isotropic eddy-viscosity model (EVM) with an extra anisotropic term. Of primary concern is how to maintain the computational stability while improving the predictive accuracy, particularly for coarse grid resolution in the near-wall region. In order to investigate the performance in detail, the proposed model is applied to numerical simulations of fully-developed plane channel flows with various grid resolutions and at various Reynolds numbers. In §2, a detailed description of the present SGS model is given. The test cases and the computational conditions are explained in §3, followed by the results and discussion in §4 and the concluding remarks in §5.

2. Turbulence Model

2.1. Basic concept of the present SGS modeling

The most frequently used method for modeling τ_{ij} in Eq. (1) is a linear EVM. Its canonical form is as follows:

$$\tau_{ij}{}^{a} = -2\nu_{SGS}S_{ij}, \quad S_{ij} = \frac{1}{2}\left(\frac{\partial \overline{U}_i}{\partial x_j} + \frac{\partial \overline{U}_j}{\partial x_i}\right), \tag{2}$$

where S_{ij} denotes the strain-rate tensor. Note that $\tau_{ij}{}^{a} = \tau_{ij} - \tau_{kk}\delta_{ij}/3$ and the SGS turbulence energy k_{SGS} is expressed as $k_{SGS} = \tau_{kk}/2$. The Smagorinsky model is representative of this category. Although introducing a linear EVM into existing CFD codes is easy, a crucial problem has been pointed out: its principal direction does not align with the real SGS-stress tensor.

Alternatively, a "scale-similarity model" can be used, for example, the well-known model proposed by Bardina et al. (1980). Among scale-similarity models, the simplest form of the SGS-Reynolds stress may be expressed as

$$\tau_{ij} = C_B\left(\overline{U}_i - \widehat{\overline{U}}_i\right)\left(\overline{U}_j - \widehat{\overline{U}}_j\right), \tag{3}$$

where $\widehat{(\ )}$ denotes a test-filtering operator and C_B is the model constant. This type of model is known to provide much better alignment with the real SGS-stress tensor (Horiuti, 1993). However, it is not always dissipative, and often makes computations unstable. To overcome this difficulty, the concept of a "mixed model" may be worth noting. This type of model is based on

the combination of the scale-similarity model (Bardina et al., 1980) and a dissipative linear EVM.

A number of research groups have proposed further advanced SGS models, the coefficients of which are determined using a dynamic procedure (see for example, Germano et al., 1991; Lilly, 1992; Zang et al., 1993; Vreman et al., 1994; Horiuti, 1997; Morinishi and Vasilyev, 2001). Every approach has provided encouraging results and useful knowledge for the further development of this field. However, the predictive performance of the current SGS models is not always adequate, particularly if they are applied to engineering applications with coarse grid resolution in the near-wall region. A further important issue is that these SGS models tend to have strong numerical instability unless some remedy is introduced to stabilize computations. Therefore, from an engineering viewpoint, providing a new modeling strategy that overcomes these severe computational problems would be a considerable contribution.

For this purpose, we start with the following representative scale-similarity model:

$$\tau_{ij}^{'} = C_B \left(\overline{U}_i - \widehat{\overline{U}}_i \right) \left(\overline{U}_j - \widehat{\overline{U}}_j \right). \tag{4}$$

Note that, for convenience in the following discussion, another notation $\tau_{ij}^{'}$ is used here for the SGS-stress tensor, although it is otherwise the same as Eq. (3). In this study, to calculate a test-filtered value $\widehat{\overline{U}}_i$, we adopt a box-type (volume-averaging-type) filtering operator, in which the filter width is twice as wide as the local grid spacing.

Next, we consider an EVM-type linear approximation for the aforementioned scale-similarity model. The following strategy may be introduced in order to evaluate an equivalent value of the eddy viscosity $\nu^{'}$:

$$\tau_{ij}^{'\,a} S_{ij} = -2\nu^{'} S_{ij} S_{ij} = -2\nu^{'} S^2 \quad \longrightarrow \quad \nu^{'} = -\frac{\tau_{ij}^{'\,a} S_{ij}}{2S^2}, \tag{5}$$

where $S^2 = S_{ij} S_{ij}$ and $\tau_{ij}^{'\,a} = \tau_{ij}^{'} - \tau_{kk}^{'} \delta_{ij}/3$. Since the production term of k_{SGS} is expressed as $-\tau_{ij}^{'} \overline{U}_{i,j}$ $(= -\tau_{ij}^{'} S_{ij})$, Eq. (5) means that this linearized approximation and the original scale-similarity model both have the same amount of energy transfer between the GS and SGS components.

Since the linear EVM $(-2\nu^{'} S_{ij})$ is recognized as an isotropic approximation for the original model $(\tau_{ij}^{'\,a})$, the following residual expression may be

useful for representing the SGS-stress anisotropy:

$$R_{ij}^{'} = \tau_{ij}^{'\,a} - \left(-2\nu^{'} S_{ij}\right), \tag{6}$$

where $R_{ij}^{'}$ is an "SGS-stress anisotropy term" that is evaluated by subtracting an EVM form from the original Bardina model. Although the linearized approximation is generally thought to contribute to computational stability, the eddy viscosity evaluated by Eq. (5) often returns a negative value. It is well known that a negative eddy viscosity is likely to cause serious computational instability. On the other hand, it is found from Eq. (5) that $R_{ij}^{'}$ yields no undesirable extra energy transfer between the GS and SGS components that may cause numerical instability under coarse-grid conditions. Therefore, if we take into account the fundamental features of Eq. (6), we may be able to successfully predict the SGS-stress anisotropy with no serious effects on the computational stability.

2.2. Proposal of a new anisotropy-resolving SGS model

Based on the above discussion, we propose a new anisotropy-resolving SGS model. The present SGS model for τ_{ij} in Eq. (1) is constructed by combining a representative isotropic EVM with an extra anisotropic term, as follows:

$$\tau_{ij} = \frac{2}{3}\, k_{SGS}\, \delta_{ij} - 2\, \nu_{SGS}\, S_{ij} + 2\, k_{SGS}\, b_{ij}^{SGS}. \tag{7}$$

In the present study, the anisotropy tensor b_{ij}^{SGS} in the extra anisotropic term of Eq. (7) is modeled as

$$b_{ij}^{SGS} = \frac{\tau_{ij}^{'} - \left(-2\nu^{'} S_{ij}\right)}{\tau_{kk}^{'} - \left(-2\nu^{'} S_{kk}\right)} - \frac{1}{3}\delta_{ij}\ , \tag{8}$$

where $\tau_{ij}^{'}$ is given by Eq. (4). As seen in Eq. (8), this anisotropy tensor b_{ij}^{SGS} takes into account the basic concept of Eq. (6) and thus is expected to reflect its fundamental features. Using Eqs. (4), (6) and (8), b_{ij}^{SGS} can be rewritten as follows:

$$\begin{aligned} b_{ij}^{SGS} &= \frac{\tau_{ij}^{'} - \left(-2\nu^{'} S_{ij}\right)}{\tau_{kk}^{'} - \left(-2\nu^{'} S_{kk}\right)} - \frac{1}{3}\delta_{ij} = \frac{\left(\frac{1}{3}\tau_{kk}^{'}\delta_{ij} + \tau_{ij}^{'\,a}\right) - \left(-2\nu^{'} S_{ij}\right)}{\tau_{kk}^{'}} - \frac{1}{3}\delta_{ij} \\ &= \frac{\tau_{ij}^{'\,a} - \left(-2\nu^{'} S_{ij}\right)}{\tau_{kk}^{'}} = \frac{R_{ij}^{'}}{\tau_{kk}^{'}}\ . \end{aligned} \tag{9}$$

As discussed earlier, $R_{ij}^{'}$ yields no undesirable extra energy transfer that may cause numerical instability. Thus, this anisotropic term is not expected to have a serious influence on the computational stability. It is also worth noting that this model has high flexibility for adopting a linear EVM in Eq. (7), and any ν_{SGS} model can be used. Note that from the form in Eq. (8), the anisotropy tensor b_{ij}^{SGS} does not depend on the model constant C_B since it appears in both the numerator and the denominator. Its effect is thus completely canceled.

Some additional explanations may be useful for understanding the present SGS modeling concept. First, this model introduces an anisotropy tensor form as shown in Eq. (8). Although this form may appear odd, this type of modeling strategy is often adopted in the field of non-linear eddy-viscosity RANS modeling (see for example, Gatski and Speziale, 1993; Craft et al., 1997; Abe et al., 1997). In fact, this form is rather advantageous for predicting the stress anisotropy with the computational stability being guaranteed. Even if the denominator approaches zero, the numerator also approaches zero mathematically at the same rate, thus always providing proper finite values for the SGS-stress anisotropy components. We also note that this form successfully guarantees the realizability of the stress anisotropy.

This extra anisotropic term is also expected to represent some characteristics of turbulent structures. Figure 1 illustrates the relation between unmodeled turbulent structures (dotted lines) and insufficient grid resolution in the near-wall region. In general, a conventional SGS model cannot model dominant eddies that are smaller than the grid width. On the other hand, a scale-similarity model can model GS eddies that are only slightly larger (dashed gray lines). Although the strength of these modeled eddies may be much weaker than expected, it is possible that these eddies, at least qualitatively, include some fundamental features of turbulent structures. If this extra anisotropic term is effective in representing these characteristics, we would expect an improvement in the predictive performance even under coarse grid conditions. In this sense, an additional strategy may be necessary to determine a relevant revel of k_{SGS} and thus a one-equation SGS model is introduced in this study.

As a first attempt, we adopt the SGS model proposed by Inagaki (2011) for the linear EVM in Eq. (7). The SGS viscosity ν_{SGS} is modeled as follows:

$$\nu_{SGS} = C_{SGS}\ f_{SGS}\sqrt{k_{SGS}}\ \Delta, \qquad f_{SGS} = 1 - \exp\left\{-\left(\frac{y_{\varepsilon}^{'}}{A_0}\right)^{4/3}\right\}, \qquad (10)$$

where C_{SGS} and A_0 are the model constants. Note that since the definition of Δ is slightly modified from what has often been used in previous studies, the model constants in Eq. (10) are slightly modified from the original ones, now being specified as $C_{SGS} = 0.05$ and $A_0 = 30$, respectively. A detailed description of Δ is provided below. In the model function f_{SGS}, the wall-distance parameter $y_\varepsilon^{'}$ is modeled as follows (Inagaki, 2011):

$$y_\varepsilon^{'} = \left(\frac{u_\varepsilon y}{\nu}\right)\sqrt{C_l \frac{y}{\Delta}}, \qquad u_\varepsilon = \left(\nu \varepsilon_{SGS}\right)^{1/4}, \tag{11}$$

where the original value of $C_l = 4$ is adopted.

In the present study, ε_{SGS} is evaluated algebraically using the following expression:

$$\varepsilon_{SGS} = C_\varepsilon \ \frac{{k_{SGS}}^{3/2}}{\Delta} + \frac{2\nu k_{SGS}}{y^2}, \tag{12}$$

with the commonly-used value of $C_\varepsilon = 0.835$. The SGS turbulence energy k_{SGS} is determined from the usual form of the transport equation as follows:

$$\frac{\mathrm{D}k_{SGS}}{\mathrm{D}t} = \frac{\partial}{\partial x_j}\left\{\left(\nu + C_k \ f_{SGS}\sqrt{k_{SGS}}\ \Delta\right)\frac{\partial k_{SGS}}{\partial x_j}\right\} - \tau_{ij}\frac{\partial \overline{U}_i}{\partial x_j} - \varepsilon_{SGS}, \tag{13}$$

with the original value of $C_k = 0.1$ (Inagaki, 2011).

As for the SGS filter width Δ, we adopt the following definition:

$$\Delta = \sqrt{\text{the maximum area among the faces of a cell.}} \tag{14}$$

In a Cartesian-structured grid system, the above definition can be rewritten as follows:

$$\Delta = \sqrt{\max\left(\Delta_x\Delta_y, \Delta_y\Delta_z, \Delta_z\Delta_x\right)}. \tag{15}$$

This definition is the same as the one introduced in a hybrid LES/RANS model by Abe (2005). The advantage of this definition is that it can exclude the effect of the grid width in the wall-normal direction, which is generally much smaller than those in the other directions near the wall. Note that using Eq. (14), we can reasonably determine Δ even in a non-orthogonal or an unstructured grid system.

This being the case, the present modeling approach is attractive from an engineering viewpoint, although there are still several remaining areas to be addressed, e.g., the effects of the Leonard and the cross terms neglected in this study. These issues are to be investigated continuously in future studies.

3. Test Cases and Computational Conditions

In order to investigate the characteristics of the present SGS model, we performed numerical simulations of fully-developed plane channel flows with various grid resolutions and at various Reynolds numbers. The computational parameters are summarized in Table 1. The Reynolds number Re_τ ($= u_\tau \delta/\nu$), based on the half channel height δ and the friction velocity, ranged from 395 to 2000. We selected the lower Re cases ($Re_\tau = 395$) for a detailed discussion of the model performance. On the other hand, the higher Re cases ($Re_\tau = 1020, 2000$) provided useful knowledge on the performance when applied to high Re turbulent flows.

An important concern is the predictive performance of this SGS model for various grid resolutions. In order to examine this issue, four grid resolutions were selected for cases at $Re_\tau = 395$, as shown in Table 1. The C395A grid resolution is recognized as being sufficient for LES. Although the C395B grid resolution is still applicable, it may be relatively coarse for LES when a simple (non-staggered) second-order central difference scheme is adopted on a finite-volume grid cell. On the other hand, the C395C grid resolution is thought to be approximately the grid resolution with which the prediction accuracy of the LES begins to clearly decrease. Finally, C395D has a much coarser grid resolution, which is usually thought to be not applicable to LES. In general, LES with such a coarse grid resolution as C395D ($\Delta z^+ \sim 80$) tends to yield a very low mean friction coefficient and results in a very poor prediction. As for the higher Re cases (C1E3 and C2E3), the grid resolution in wall unit was set to be similar to that of C395C (i.e., $\Delta z^+ = 40$–50).

Calculations were performed using an unstructured finite-volume procedure that was almost the same as that used in Muto et al. (2012). This method used vertex-centered type storage on a grid. The second-order central difference scheme was used to discretize the spatial derivatives, except for the convection term of k_{SGS} (Eq. (13)), which was discretized by the second-order upwind scheme. Note that a rectangular-grid system was used in the present channel-flow simulation, and thus the predictive performance was actually equivalent to that of a collocated structured grid system that used a discretization scheme at the same level.

The time marching was based on the fractional step method (Kim and Moin, 1985), in which the second-order Crank-Nicolson scheme was used for the velocity equations (Eq. (1)). On the other hand, concerning the transport equation of k_{SGS}, the first-order Euler implicit scheme was used. The source

terms appearing in these equations were basically treated explicitly with the first-order time accuracy, except for the dissipation term in the k_{SGS} equation that was treated implicitly with a linearization manner in time for stable computation. The coupling of the velocity and pressure fields was based on the simplified marker and cell (SMAC) method (Amsden and Harlow, 1970). The flow rate on the control-volume surface was estimated using the Rhie-Chow interpolation (Rhie and Chow, 1983). In all of the test cases, the Courant number for the time steps was set to be less than 1.0. For the boundary conditions, the periodic condition was imposed in the streamwise and spanwise directions, whereas the no-slip conditions were specified at the walls, with the wall-nearest node being placed at $y^+ < 1$, as shown in Table 1. Since some first-order treatments in the time marching were adopted in this study, we conducted additional simulations with the time step in Table 1 being reduced to half. The obtained results are summarized in the Appendix. From comparison of the simulation results shown below with those in the Appendix, we see that the time-integration scheme does not give any crucial effect on the present computational results.

As summarized in Table 2, in order to more fully explore the model performance, we performed the following additional computations (besides the present anisotropic one-equation SGS model, listed as "A1E" in Table 2):

- Four cases (C395A, C395B, C395C and C395D in Table 1) that used the original isotropic one-equation SGS model (without the extra anisotropic term, listed as "I1E" in Table 2).
- Four cases using a dynamic Smagorinsky model (Germano et al., 1991; Lilly, 1992) (listed as "DSM" in Table 2).
- Two cases (C395A and C395B) with no SGS model being used (listed as "NO" in Table 2).

Note that besides these SGS models, we also attempted to perform simulations with the original Bardina model shown in Eq. (3) and a mixed SGS model, in which Eq. (3) (instead of the present extra anisotropic term) was directly added to a linear SGS model. However, the computations using the Bardina model and the mixed SGS model suffered from strong numerical instability, and we could not obtain the final simulation results. Some investigations of the equivalent eddy viscosity evaluated from the Bardina model (Eq. (5)) indicated that the evaluated values often become negative instantaneously at many grid nodes. This basic feature must cause computational

instability. In this sense, the present modified anisotropic term in Eq. (7) contributes to making computations stable by excluding such an undesirable effect. This may be one reason why the present anisotropic SGS model is rather stable compared with these conventional SGS models.

As for the computations with the dynamic Smagorinsky model, a conventional linear model expression (Germano et al., 1991; Lilly, 1992) was used. Note that such a dynamic SGS model generally shows strong numerical instability. Since the computations with the dynamic SGS model quickly diverged, we introduced a well-known strategy of clipping the negative values of ν_{SGS}. Although stable computations were thereby achieved by clipping negative ν_{SGS}, we must keep it in mind that the effect of the backward scattering was no longer included in the computational results. Finally, concerning the calculations with no SGS model, computational results were obtained only for C395A and C395B. For the other cases, i.e., C395C and C395D, the computations were numerically unstable and results could not be obtained, probably due to grid resolution being too coarse in the near-wall region.

4. Results and Discussion

4.1. Predictive performance of existing SGS models

First, in order to discuss the performance of an existing SGS model, the mean-velocity distributions predicted by the dynamic Smagorinsky model ("DSM" in Table 2) for various grid resolutions at $Re_\tau = 395$ are compared with the DNS data (Moser et al., 1999) in Fig. 2. The prediction accuracy becomes worse as the grid resolution becomes coarser. Generally speaking, an important advantage of a dynamic SGS model is the potential ability to reproduce both the forward scattering and the backward scattering (Germano et al., 1991; Lilly, 1992; Horiuti, 1997; Morinishi and Vasilyev, 2001). This notable feature is expected to work properly if the grid resolution is sufficiently fine. However, it is difficult to successfully reproduce both directions of scattering when using a coarse grid. As discussed above, to avoid the numerical instability caused by the original dynamic SGS model, we clipped the ν_{SGS} values that were negative. This stabilizes the computations but makes them more dissipative, which results in considerable up-shift in the mean-velocity predictions for the coarser grid cases.

Next, to confirm the performance of the original SGS model, Fig. 3 shows the mean-velocity distributions predicted by the original isotropic one-equation SGS model without the extra anisotropic term ("I1E" in Table 2).

It is readily seen that the prediction accuracy becomes worse as the grid resolution becomes coarser. This trend is similar to what was seen in Fig. 2. As discussed above, the grid resolutions of C395C ($\Delta z^+ = 40$) and C395D ($\Delta z^+ = 80$) are generally thought to be too coarse for LES, and thus such a grid-dependent trend appears to be a natural consequence.

4.2. Predictive performance of the present anisotropic SGS model

We now consider the predictive performance of the present anisotropic one-equation SGS model ("A1E" in Table 2). Figure 4 shows the distributions of the mean velocity predicted by this model for various grid resolutions at $Re_\tau = 395$. The accuracy of predicting the mean velocity is considerably improved compared to those by the original isotropic one-equation SGS model shown in Fig. 3. The computational results for all grid resolutions generally correspond well to those of the DNS data, although slight underpredictions are observed in the logarithmic region. A reasonable prediction of the mean velocity also provides a good prediction of the skin friction coefficient. Such a grid-independent trend in the mean-velocity distributions for a wide range of computational conditions is very encouraging, and indicates that this model will be successfully applied to more complex and practical LES in future studies.

In order to clarify the effect of the numerical scheme adopted in the CFD code, the mean-velocity distributions obtained from the results with no SGS model ("NO" in Table 2) are compared in Fig. 5 with those by other SGS models. Concerning the results for C395A, all the predictions correspond generally well to the DNS data, although slight differences are seen in the distributions. On the other hand, the results for C395B may indicate a slight dissipative feature even in the mean-velocity distribution with no SGS model. Unlike the discussion on RANS modeling, assessing the predictive performance of an LES model is likely to include many factors. In a notable study, Morinishi and Vasilyev (2001) investigated the computational results when using no SGS model. They adopted fully conservative higher-order difference schemes (mainly the fourth-order scheme) for their detailed discussion because they indicated that the truncation error of the second-order difference scheme may act as an effective SGS stress. Considering the fact that the present study adopted an average-level second-order central difference scheme, some up-shift in the mean-velocity predictions for C395B may be inevitable. Although the calculations with no SGS model for the other cases suffered from numerical instability due to too coarse grid resolution in the

near-wall region, a feature qualitatively similar to that found by Morinishi and Vasilyev (2001) is seen in the results at least for C395A and C395B.

On the other hand, another notable feature is seen in the results from the present anisotropic one-equation SGS model. It is seen in Fig. 5 (b) that the prediction of the mean velocity is improved even for C395B, for which we see some down-shift compared with the results with no SGS model. In general, the SGS model works as an additional viscosity that leads to an up-shift in the mean-velocity prediction. In this sense, the present results seem to show an unfamiliar feature. However, this unfamiliar feature may indicate an important advantage of the present SGS model. It is thought that the introduction of a one-equation SGS model contributes to an improvement in the predictive performance. Considering this fact together with the statistics for turbulence, shown below, we see that the present SGS model actually works as a kind of detached-eddy simulation (DES) model as the grid resolution becomes coarser.

The computational results for the Reynolds shear stress predicted by the present anisotropic one-equation SGS model are presented in Fig. 6. Although the balance of the GS and SGS parts is largely different between the various test cases, the distributions of the total (resolved+modeled) values coincide with each other and are in good agreement with the DNS data. This is a natural consequence of accurate prediction of the mean velocity, as shown in Fig. 4. Figure 7 presents the distributions of the turbulence energy predicted by the present anisotropic SGS model. As the grid resolution becomes coarser, the SGS component of the turbulence energy increases, and the GS component decreases. Although some overpredictions appear in the total turbulence energy for the coarser grid cases, the locations of the peak values are predicted sufficiently well, resulting in a trend that corresponds generally well to that of the DNS data.

Figure 8 shows the total turbulence intensities predicted by the present anisotropic SGS model. Note that the values in the figure were obtained from the root-mean square of the total Reynolds normal stresses. All of the components are predicted generally well, although a close inspection of the results reveals that the discrepancy of the prediction increases as the grid resolution becomes coarser. In this respect, there remains some margin for improvement.

The near-wall behavior of the predicted turbulence for C395B is shown in Fig. 9. Figures 9 (a) and (b) show that a reasonable trend of the near-wall behavior is obtained for both the turbulence energy and the Reynolds shear

stress. Not only the GS component but also the SGS component provide the correct behaviors, resulting in reasonable predictions for the total values. It is also found from Fig. 9 (c) that the total turbulence intensities are reasonably predicted for all of the components. Although the present SGS model introduces some empirical factors into the model functions, it is considered that they properly work to provide a reasonable behavior of the near-wall turbulence.

As such, the predictive performance of the present anisotropic one-equation SGS model is generally acceptable. Therefore, the proposed SGS model may have the potential to be used with a wide range of grid resolutions.

4.3. Higher Reynolds-number cases

Figure 10 compares the mean-velocity predictions obtained by the original isotropic and the proposed anisotropic one-equation SGS models for higher Re cases ($Re_\tau = 1020$, 2000). As shown in Fig. 10 (a), the original isotropic one-equation SGS model produces considerable overpredictions, where the results shift upward from the generally-accepted log-law line, i.e., $\overline{U}^+ = (1/0.41)\log y^+ + 5.0$. This is a well-known feature when LES is applied to coarse grid resolutions.

On the other hand, the trend for the proposed anisotropic one-equation SGS model is clearly different from that for the isotropic SGS model. The proposed model generally returns reasonable predictions of the mean velocity for all Re cases. In general, this indicates that the prediction accuracy in the near-wall region is improved, and thus it is expected that the mean-friction coefficient is reasonably predicted.

In order to discuss the model performance in more detail, Fig. 11 shows the results at $Re_\tau = 1020$ that were obtained by the present SGS model and the corresponding DNS data obtained by Abe et al. (2004). We can see in Fig. 11 (a) that the mean velocity is generally predicted well, although a slight underprediction is still seen in the logarithmic region. Considering the coarse grid resolution as shown in Table 1, the predictive performance of the present SGS model is worth noting, though such a down-shift is to be improved for further accurate predictions. As seen in Fig. 11 (b), the computational results of the Reynolds shear stress correspond well to the DNS data. The total turbulence intensities are compared in Fig. 11 (c), where all of the components are generally predicted well. Although some discrepancies are still seen, the present results are thought to be encouraging under such a coarse grid resolution.

On the other hand, it is well known that the prediction of the mean velocity is directly related to the Reynolds shear-stress distribution in the case of a plane channel flow. In this sense, a very close inspection of the total Reynolds shear-stress prediction in Fig. 11 (b) may indicate a slight overprediction in the region far from the wall compared with the DNS data. The discrepancy in the mean-velocity profile shown in Fig. 11 (a) is actually caused by this slight difference in the total Reynolds shear-stress prediction in the logarithmic region. Therefore, further detailed investigations are necessary to improve such slight underpredictions of the mean velocity. However, since this issue may include many factors to be considered, it will be left as an area of future study.

5. Concluding Remarks

An improved subgrid-scale (SGS) model was proposed by combining an isotropic linear eddy-viscosity term with an extra anisotropic term. Of primary interest in the present study was how to maintain computational stability while improving the predictive performance particularly for coarse grid resolution in the near-wall region. For the extra anisotropic term, we introduced a residual term after subtracting an eddy-viscosity form from the Bardina's SGS-Reynolds-stress model. The resultant extra term yields no undesirable extra energy transfer between the GS and SGS components that could cause numerical instability under coarse grid conditions. Therefore, this extra term is not expected to adversely affect the computational stability.

In order to examine the model performance, the proposed SGS model was applied to numerical simulations of fully-developed plane channel flows with various grid resolutions and at various Reynolds numbers. Compared to the original isotropic one-equation SGS mode, the computational results were considerably improved. In particular, the mean velocity was successfully predicted for cases of coarser grid resolution, and the grid dependence was considerably reduced. These findings indicate the usefulness of the present SGS model for engineering applications.

Finally, we briefly note the following as areas of future study. In order to cover a wide range of computational conditions including severely coarse grid resolutions in the near-wall region, the present SGS model introduces several empirical factors into the model functions and the transport equation for k_{SGS}. Therefore, regarding these factors, there may still remain several

points to be discussed and improved. Although the predictive performance of the present SGS model is generally acceptable, more detailed discussion will contribute to further development.

Acknowledgments

This research was partially supported by Grant-in-Aid for Scientific Research 24560197, sponsored by the Japan Society for the Promotion of Science. The present computation was mainly carried out using the computer facilities at Research Institute for Information Technology, Kyushu University, Japan.

Appendix

In order to confirm the effect of the time-integration methods used in the present study on the simulation results, we conducted additional simulations with the time step being half of that used in Table 1. The mean-velocity predictions by the present anisotropic SGS model are shown in Fig. 12. The fundamental features of the predictions are very similar to those shown in Fig. 4. Next, Fig. 13 shows the predictions of the total turbulence intensities. We see that the distributions of these turbulent statistics correspond well to those shown in Fig. 8. From these comparisons, it is clear that the time-integration scheme has no crucial negative effects on the results.

References

Abe, H., Kawamura, H., and Matsuo, Y. (2004). Surface heat-flux fluctuations in a turbulent channel flow up to Re_τ=1020 with Pr=0.025 and 0.71. *Int. J. Heat Fluid Flow*, **25**, 404-419.

Abe, K., Kondoh, T., and Nagano, Y. (1997). On Reynolds stress expressions and near-wall scaling parameters for predicting wall and homogeneous turbulent shear flows. *Int. J. Heat Fluid Flow*, **18**, 266-282.

Abe, K. (2005). A hybrid LES/RANS approach using an anisotropy-resolving algebraic turbulence model. *Int. J. Heat Fluid Flow*, **26**, 204-222.

Amsden, A.A., and Harlow, F.H. (1970). A simplified MAC technique for incompressible fluid flow calculations. *J. Comput. Phys.*, **6**, 322-325.

Bardina, J., Ferziger, J.H., and Reynolds, W.C. (1980). Improved subgrid scale models for large eddy simulation. *AIAA Paper*, **80-1357**.

Craft, T.B., Launder, B.E., and Suga, K. (1997). Prediction of turbulent transitional phenomena with a nonlinear eddy viscosity model. *Int. J. Heat Fluid Flow*, **18**, 15-28.

Gatski, T.B., and Speziale, C.G. (1993). On explicit algebraic stress models for complex turbulent flows. *J. Fluid Mech.*, **254**, 59-78.

Germano, M., Piomelli, U., Moin, P., and Cabot, W.H. (1991). A dynamic subgrid-scale eddy viscosity model. *Phys. Fluids*, **A3**, 1760-1765.

Horiuti, K. (1993). A proper velocity scale for modeling subgrid-scale eddy viscosities in large eddy simulation. *Phys. Fluids A*, **5**, 146-157.

Horiuti, K. (1997). A new dynamic two-parameter mixed model for large-eddy simulation. *Phys. Fluids*, **9**, 3443-3464.

Inagaki, M. (2011). A new wall-damping function for large eddy simulation employing Kolmogorov velocity scale. *Int. J. Heat Fluid Flow*, **32**, 26-40.

Kim, J., and Moin, P. (1985). Application of a fractional-step method to incompressible Navier-Stokes equations. *J. Comput. Phys.*, **59**, 308-323.

Lilly, D.K. (1992). A proposed modification of the Germano subgridscale closure method. *Phys. Fluids A*, **4**, 633-635.

Morinishi, Y., and Vasilyev, O.V. (2001). A recommended modification to the dynamic two-parameter mixed subgrid scale model for large eddy simulation of wall bounded turbulent flow. *Phys. Fluids*, **13**, 3400-3410.

Moser, R.D., Kim, J., and Mansour, N.N. (1999). Direct numerical simulation of turbulent channel flow up to Re_τ=590. *Phys. Fluids*, **11**, 943-945.

Muto, M., Tsubokura, M., and Oshima, N. (2012). Negative Magnus lift on a rotating sphere at around the critical Reynolds number. *Phys. Fluids*, **24**, 014102.

Rhie, C.M., and Chow, W.L. (1983). Numerical study of the turbulent flow past an airfoil with trailing edge separation. *AIAA J.*, **21**, 1525-1532.

Vreman, B., Geurts, B., and Kuerten, H. (1994). On the formulation of the dynamic mixed subgrid-scale model. *Phys. Fluids*, **6**, 4057-4059.

Zang, Y., Street, R.L., and Koseff, J.R. (1993). A dynamic mixed subgrid-scale model and its application to turbulent recirculating flows. *Phys. Fluids A*, **5**, 3186-3196.

Table 1: Computational conditions for channel-flow cases.

Case	Re_τ	Grid numbers	Domain (x-z)	Δx^+	Δy^+	Δz^+	Δt
C395A	395	$61 \times 61 \times 61$	$6\delta \times 1.5\delta$	40	0.8–36	10	1×10^{-3}
C395B	395	$31 \times 61 \times 31$	$6\delta \times 1.5\delta$	80	0.8–36	20	1×10^{-3}
C395C	395	$31 \times 61 \times 31$	$12\delta \times 3\delta$	160	0.8–36	40	1×10^{-3}
C395D	395	$31 \times 61 \times 31$	$12\delta \times 6\delta$	160	0.8–36	80	1×10^{-3}
C1E3	1020	$41 \times 81 \times 41$	$6\delta \times 1.5\delta$	152	0.7–78	38	5×10^{-4}
C2E3	2000	$61 \times 91 \times 61$	$6\delta \times 1.5\delta$	200	0.8–148	50	5×10^{-4}

Table 2: Subgrid-scale models used in the present study.

Case	SGS model
A1E	The present anisotropic 1-Eq. SGS model
I1E	Original isotropic 1-Eq. SGS model
DSM	Dynamic Smagorinsky model
NO	No SGS model

Figure captions

1 Schematic image of the relation between unmodeled eddies (dotted lines) and slightly larger GS eddies (dashed gray lines) in the near-wall region.
2 Distributions of the mean velocity predicted by the dynamic Smagorinsky model (DSM).
3 Distributions of the mean velocity predicted by the original isotropic one-equation SGS model (I1E).
4 Distributions of the mean velocity predicted by the present anisotropic one-equation SGS model (A1E).
5 Comparison of mean-velocity distributions for C395A and C395B.
6 Profiles of Reynolds shear stress predicted by the present anisotropic SGS model (A1E).
7 Profiles of turbulence energy predicted by the present anisotropic SGS model (A1E).
8 Distributions of total turbulence intensities predicted by the present anisotropic SGS model (A1E).
9 Near-wall behavior of turbulence obtained by the present anisotropic SGS model (C395B-A1E).
10 Comparison of mean-velocity distributions for cases with higher Reynolds numbers.
11 Comparison of computational results by the present anisotropic one-equation SGS model (C1E3-A1E).
12 Mean-velocity distributions predicted by the present anisotropic one-equation SGS model with the time step cut in half (A1E).
13 Distributions of total turbulence intensities predicted by the present anisotropic SGS model with the time step cut in half (A1E).

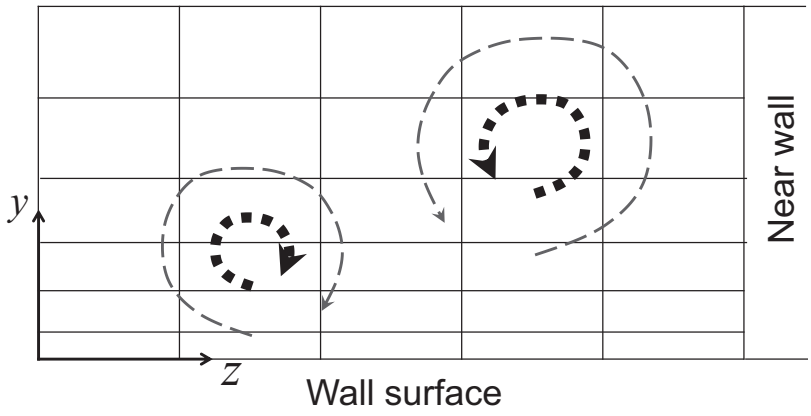

Figure 1: Schematic image of the relation between unmodeled eddies (dotted lines) and slightly larger GS eddies (dashed gray lines) in the near-wall region.

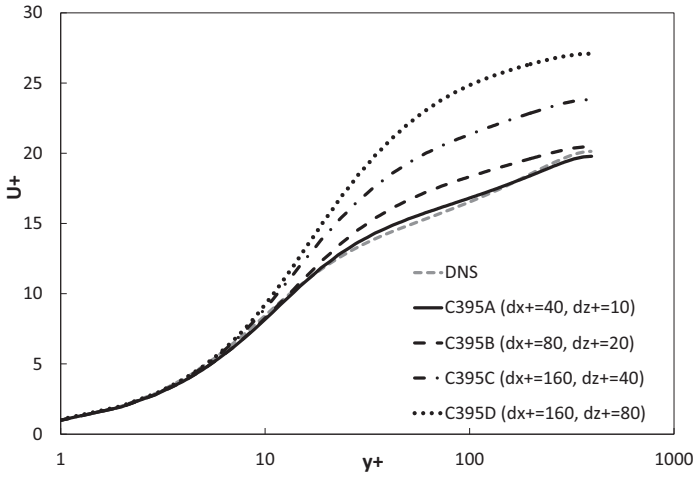

Figure 2: Distributions of the mean velocity predicted by the dynamic Smagorinsky model (DSM).

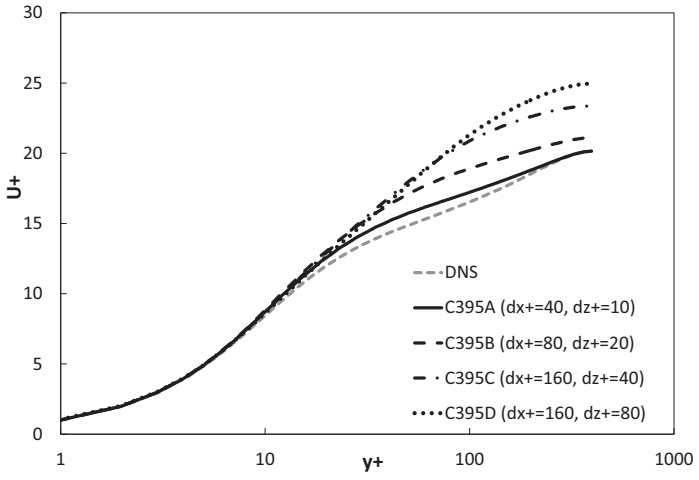

Figure 3: Distributions of the mean velocity predicted by the original isotropic one-equation SGS model (I1E).

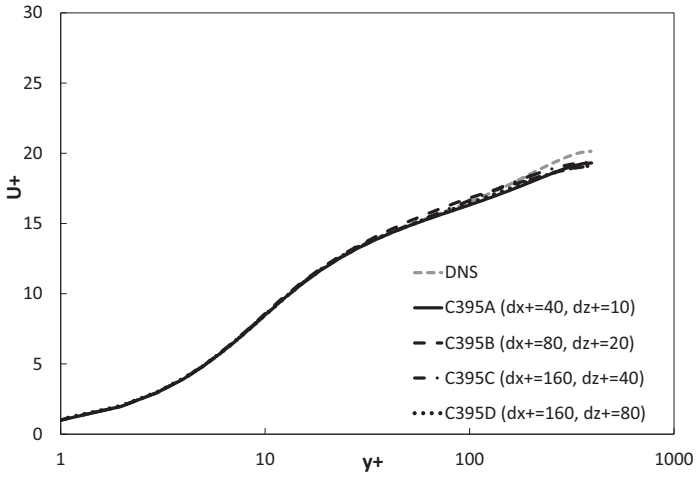

Figure 4: Distributions of the mean velocity predicted by the present anisotropic one-equation SGS model (A1E).

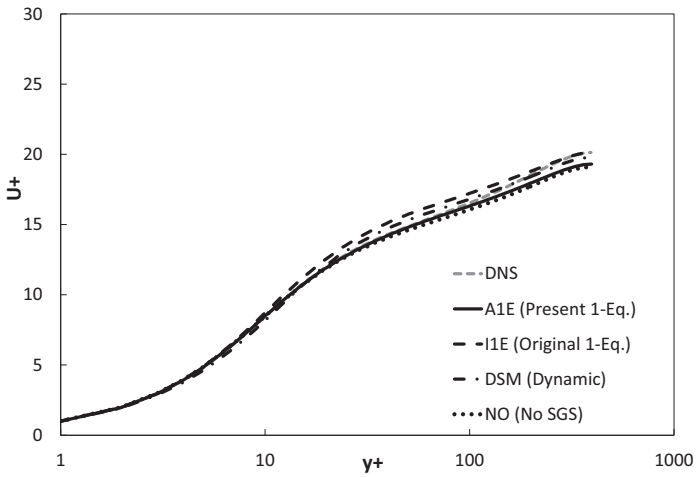

(a) C395A

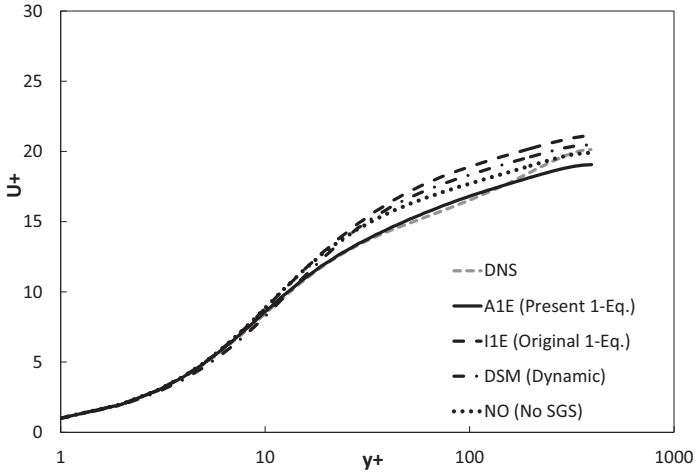

(b) C395B

Figure 5: Comparison of mean-velocity distributions for C395A and C395B.

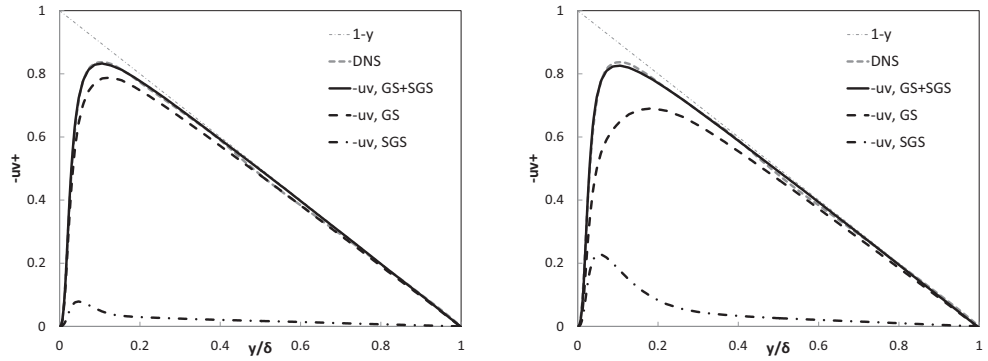

(a) C395A (b) C395B

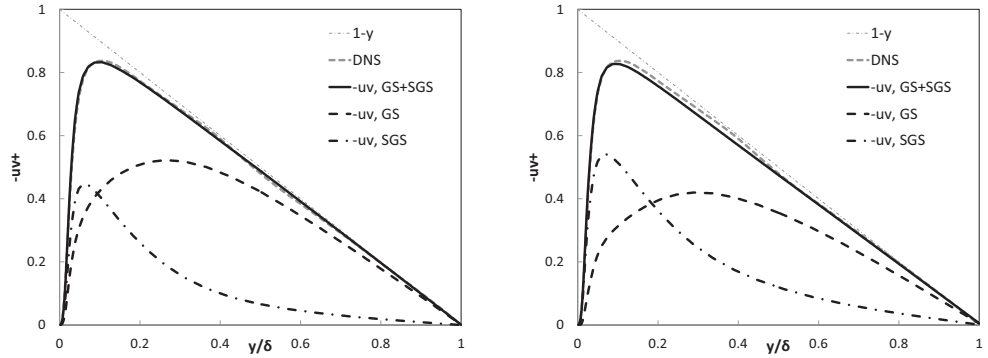

(c) C395C (d) C395D

Figure 6: Profiles of Reynolds shear stress predicted by the present anisotropic SGS model (A1E).

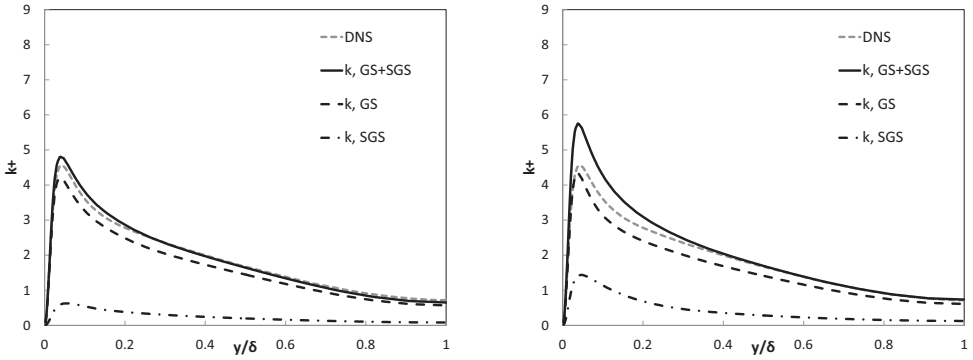

(a) C395A (b) C395B

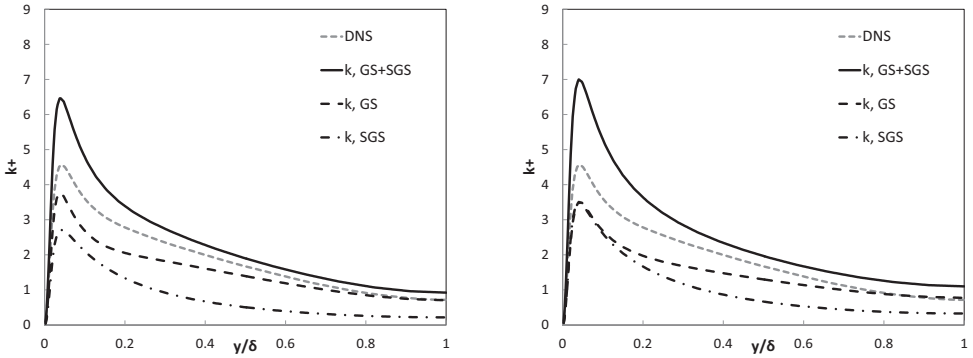

(c) C395C (d) C395D

Figure 7: Profiles of turbulence energy predicted by the present anisotropic SGS model (A1E).

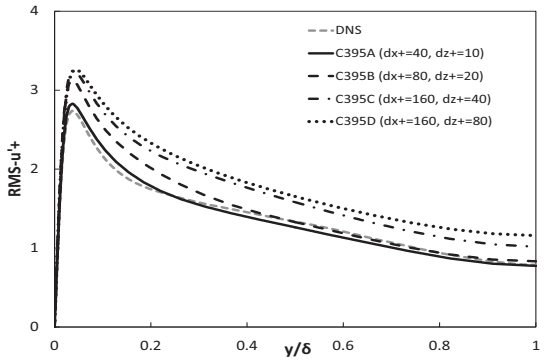

(a) Streamwise direction

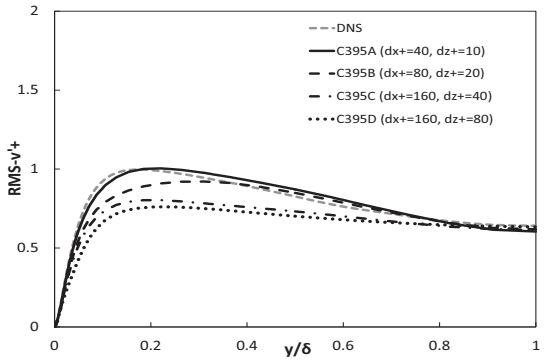

(b) Wall-normal direction

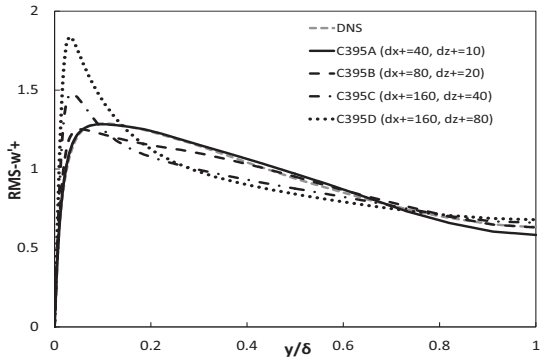

(c) Spanwise direction

Figure 8: Distributions of total turbulence intensities predicted by the present anisotropic SGS model (A1E).

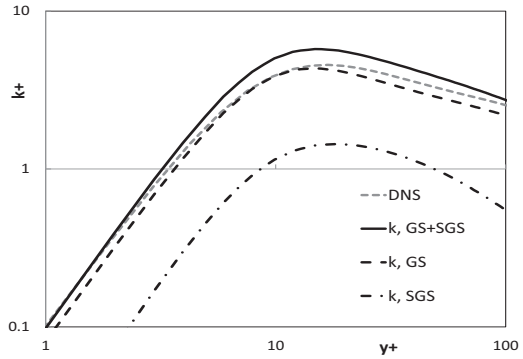

(a) Turbulence energy

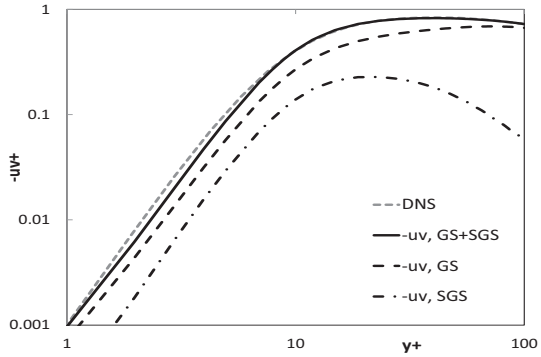

(b) Reynolds shear stress

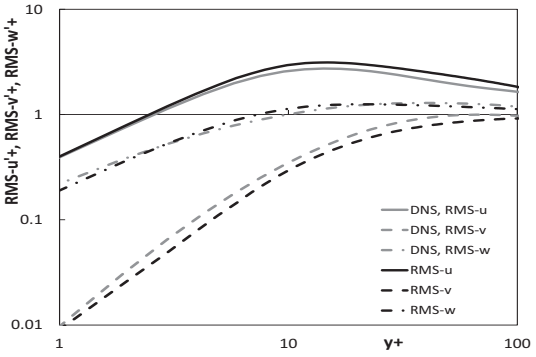

(c) Total turbulence intensities

Figure 9: Near-wall behavior of turbulence obtained by the present anisotropic SGS model (C395B-A1E).

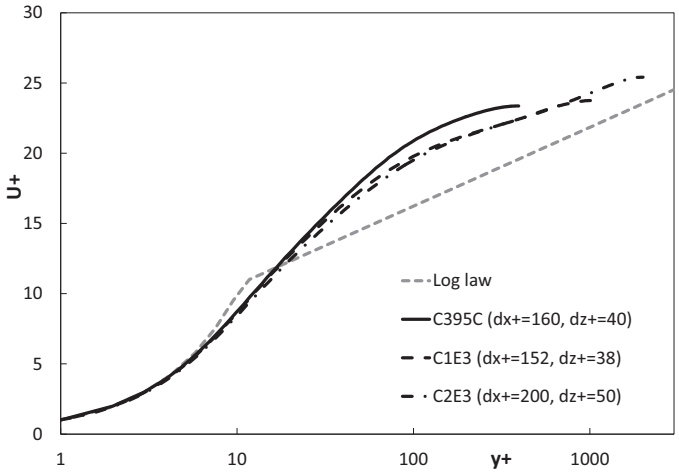

(a) The original isotropic one-equation SGS model (I1E)

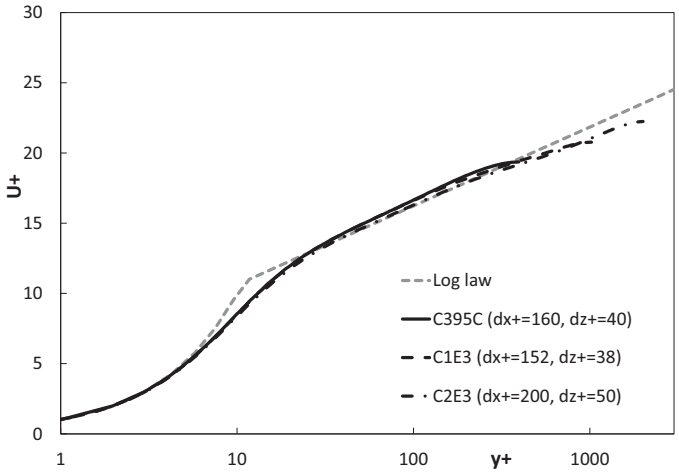

(b) The present anisotropic one-equation SGS model (A1E)

Figure 10: Comparison of mean-velocity distributions for cases with higher Reynolds numbers.

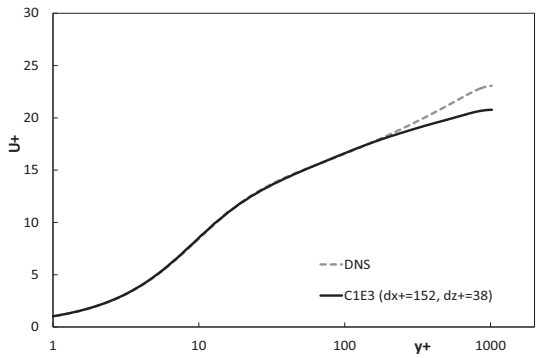

(a) Mean velocity

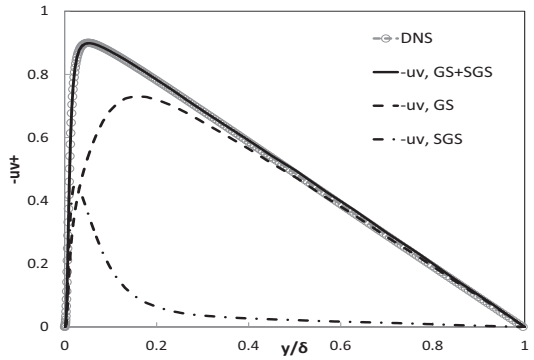

(b) Reynolds shear stress

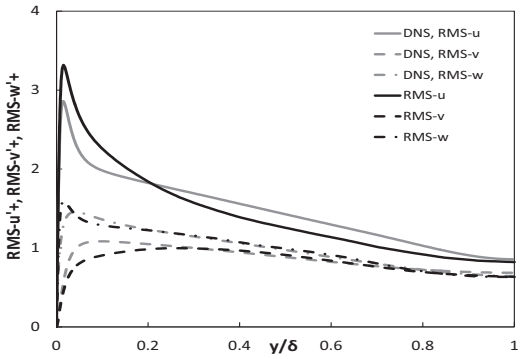

(c) Total turbulence intensities

Figure 11: Comparison of computational results by the present anisotropic one-equation SGS model (C1E3-A1E).

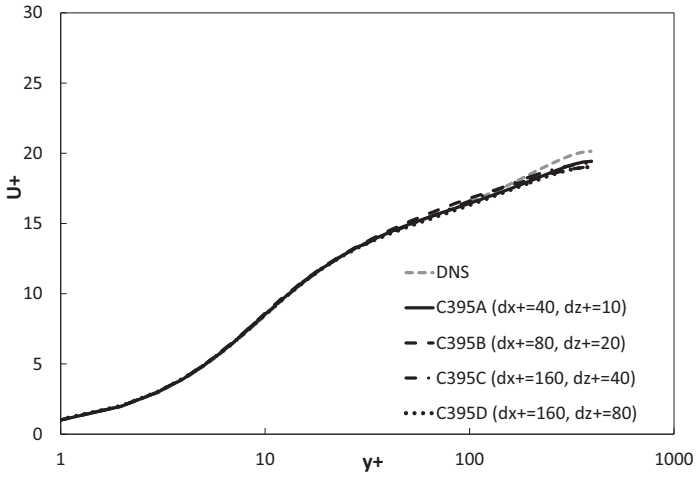

Figure 12: Mean-velocity distributions predicted by the present anisotropic one-equation SGS model with the time step cut in half (A1E).

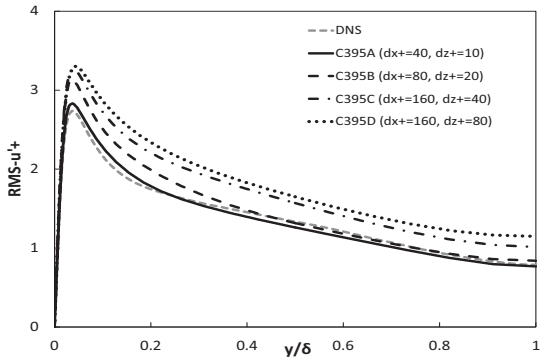

(a) Streamwise direction

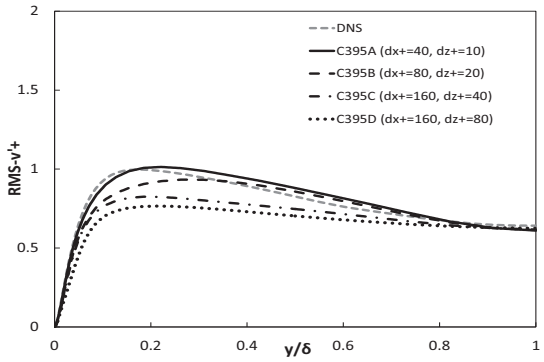

(b) Wall-normal direction

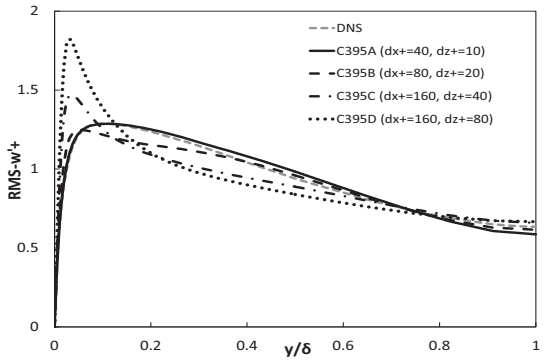

(c) Spanwise direction

Figure 13: Distributions of total turbulence intensities predicted by the present anisotropic SGS model with the time step cut in half (A1E).